PRESSURE MEASUREMENTS IN OSCILLATORY NACA0012 AIRFOIL - EXPERIMENTAL AND COMPUTATIONAL RESULTS

Ana Paula Franco Bueno, apaula.bueno@uol.com.br
José Laércio Doricio, josedoricio@yahoo.com.br
Antônio Carlos Henriques Marques, achm@sc.usp.br
Igor Braga de Paula, igorbra@gmail.com
Fernando Martini Catalano, catalano@sc.usp.br
Paulo Celso Greco Júnior, pgreco@sc.usp.br
Departamento de Engenharia de Materiais, Aeronáutica e Automobilística
Escola de Engenharia de São Carlos - Universidade de São Paulo
Av. Trabalhador São-Carlense, 400 - Centro - CEP: 13560-970 - São Carlos - São Paulo - Brasil.

Abstract. *This work reports on experimental and numerical study of a NACA0012 airfoil with angular oscillation. Experimental tests were performed in an open-circuit wind tunnel in order to measure the pressure distribution acting on that airfoil. The pressure distribution was measured using 24 pressure taps placed along the airfoil surface. The angular oscillation was obtained with an electrical motor coupled to the airfoil. The mean flow velocity was kept constant during the experiment and the airfoil oscillation frequencies were set to 0.5 Hz and 2 Hz. The airfoil incidence angle varied from 0^o to 30^o. The data acquisition from the pressure signals was synchronized with the airfoil oscillation. The results show a dynamic stall behavior. A free-slip computational approach of the Immersed Boundary Method was used to simulate the inviscid compressible flow modelled by the Euler equations. The Finite Differences Method was used, in a structured mesh, to solve the governing equations. The fourth order Runge-Kutta method was employed for time integration, and the second order Steger-Warming method with Min-Mod flux limiter is employed for spatial discretization. The results obtained by the computational study showed the applicability of the free-slip immersed boundary method to the unsteady airfoil case.*

Keywords: *Pressure measurements, unsteady regime, oscillating airfoil, Immersed Boundary Method, dynamic stall.*

1. INTRODUCTION

An increasing interest on the development of computational models for aerodynamic studies is motivated by their inherent flexibility, controlability and by the evolution of computers. Forced oscillation techniques have been widely used to determine aerodynamic stability characteristics for wings in wind tunnel, including dynamic stall. Dynamic stall is a phenomenon that affects airfoils, wings, and rotors in unsteady flows. It is due to changes, periodic or not, in the inflow conditions and/or angle of attack. In some cases, such rotorcrafts in forward flight, dynamic stall is intrinsic to their state of operation. A comprehensive review of CFD methods for dynamic stall has been published by Coton and Galbraith (1999), McCroskey et al. (1976), Niven and Galbraith (1997), and Carta (1974). In wind turbines, it is the result of atmospheric turbulence, wind shears, earth boundary layer, etc. The aerodynamic characteristics are affected and depend of the frequency and amplitude of motion, and the point of operation. Other factors affecting dynamic stall are the Reynolds and Mach numbers, and the geometrical shape. There are other, maybe minor factors, like the vortex effects, blade flapping and bending, etc. A pitching motion induces a periodic variation of the angle of attack. When the oscillation occurs around a mean angle of attack close to C_{Lmax} (static stall) the viscous effect become predominant. However, the large scale separation is largely an inviscid problem (Filippone and Sorensen, 1995). The description of the physical events taking place is far more difficult. Dynamic stall phenomenon can be identified by the hysteresis (these effects change with the reduced frequency), Filippone and Sorensen (1995). Despite of the important viscous effects, the computational simulations, with compressible homogeneous and inviscid flow, presented qualitatively compatible results with the dynamic stall features.

Theoretical studies have demonstrated that inviscid separation (recirculation) can occur in rotational flows as a result of the premature retardation of the surface velocity caused by vorticity in the flow. Insviscid “separation” has been observed in numerical calculations of flow past circular cylinders (Kumar and Salas, 1985), circular cones (Marconi, 1983), delta wings (Raj and Sikora, 1984), and airfoils (Barton and Pulliam, 1984). Actual fluid flow is never truly inviscid, although in some cases the viscous effects are negligible. Many of the works reported in the literature, the accuracy of the results is quite good, and the solutions obtained are representative of the physical flow of interest (Barton and Pulliam, 1984). There are a number of physical phenomena which cause flow separation and recirculation. In all cases, in which recirculation is present, vorticity must also be present, and thus there must exist some mechanism which generates vorticity. The question naturally arises as to the physical interpretation of these flows in the absence of physical viscosity (Barton and Pulliam, 1984). Forced oscillation techniques can also be applied as a method of system identification, similar to the collection

of flight test data. In case of forced oscillation, disturbances are not induced by the variation of the flight condition as performed in traditional flighting tests (Carta, 1974). In the forced case, the perturbations are caused by the oscillatory movements of the airfoil. This work presents the study of a forced oscillation of an airfoil NACA0012 to determine the airfoil aerodynamic characteristics.

The test setup consists of a mechanism to oscillate the wing along a single pitch axis at chosen amplitudes and frequencies. Initial tests show that the forced oscillation process returns results which match with the expected trends. The aerodynamic measurements of pressure, drag, lift, and moment for non-stationary regimes in wind tunnel can be used for verification of the results obtained by computational simulations. In non-stationary regimes, the airfoil profile oscillates performing periodic movements around a mean angle of attack. This movements can be of rotation or translation type. The forced oscillation test is a feasible method to determine the aerodynamic parameters of airfoils and to help to adjust and validate procedures of numerical methods. In the current study, the pressure coefficient, C_p, and the normal force coefficient C_N values were analyzed. The forced oscillation test is performed using an experimental process and a computational simulation. The results are compared and the singularities are captured, in special the dynamic stall phenomenon.

2. METHODOLOGY

The methodology used in this work is composed of two approaches. One consists in an experimental investigation and the other is a numerical simulation of the aerodynamic of an oscillatory airfoil. Both approaches are performed at similar conditions in order to enable the comparison of the results. These comparisons are presented and discussed.

2.1 EXPERIMENTAL PROCEDURE

The experimental setup (Fig. 2) consists of a standard test which is capable to produce a forced sinusoidal perturbation in angular motion. Only one degree of freedom was chosen in order to simplify the development and analysis of the forced oscillation test procedure. The open circuit wind tunnel used (Fig. 1) has test section with $0.3 \times 0.4m^2$. The turbulence level of this tunnel in the range of $10 - 5000Hz$ is close to 0.1% of the free stream velocity. The airfoil model was a NACA0012 profile, built with expanded polystyrene and wood with dimensions of $0.15m$ of chord and $0.26m$ of span. 24 pressure taps were placed along the centerline of the wing with a chordwise spacing of $0.01m$ between each hole, as shown in Fig. 3. Short tubes ($452mm$ of length, and $1mm$ in diameter) were used to minimize delay of the signals in the measurements. The pressure along the airfoil chord was measured with a scanivalve system controlled by the Lab View system. The airfoil section was couplet to a DC motor. This configuration was capable to produce a forced sinusoidal pitch oscillation of the airfoil incidence angle. Just one degree of freedom was covered in the measurements in order to simplify the set-up and facilitate the analysis of the results.

Figure 1. LAE wind tunnel with test section.

The delay of the pressure signal was assumed to be negligible within the range of airfoil oscillation frequencies covered in the current experiments. This simplification was adopted for this preliminary work. However, in a more detailed investigation it is necessary to perform a dynamic calibration of the system. A device for such type of calibration is being developed and would be used in future works. The pressure transducer used was a single channel Scanivalve device with a full measurement range of $1psi$. The readings from all the 24 pressure taps plus the static and total pressures at the test section were obtained by multiplexing the sensor input. The output from the pressure transducer was digitalized

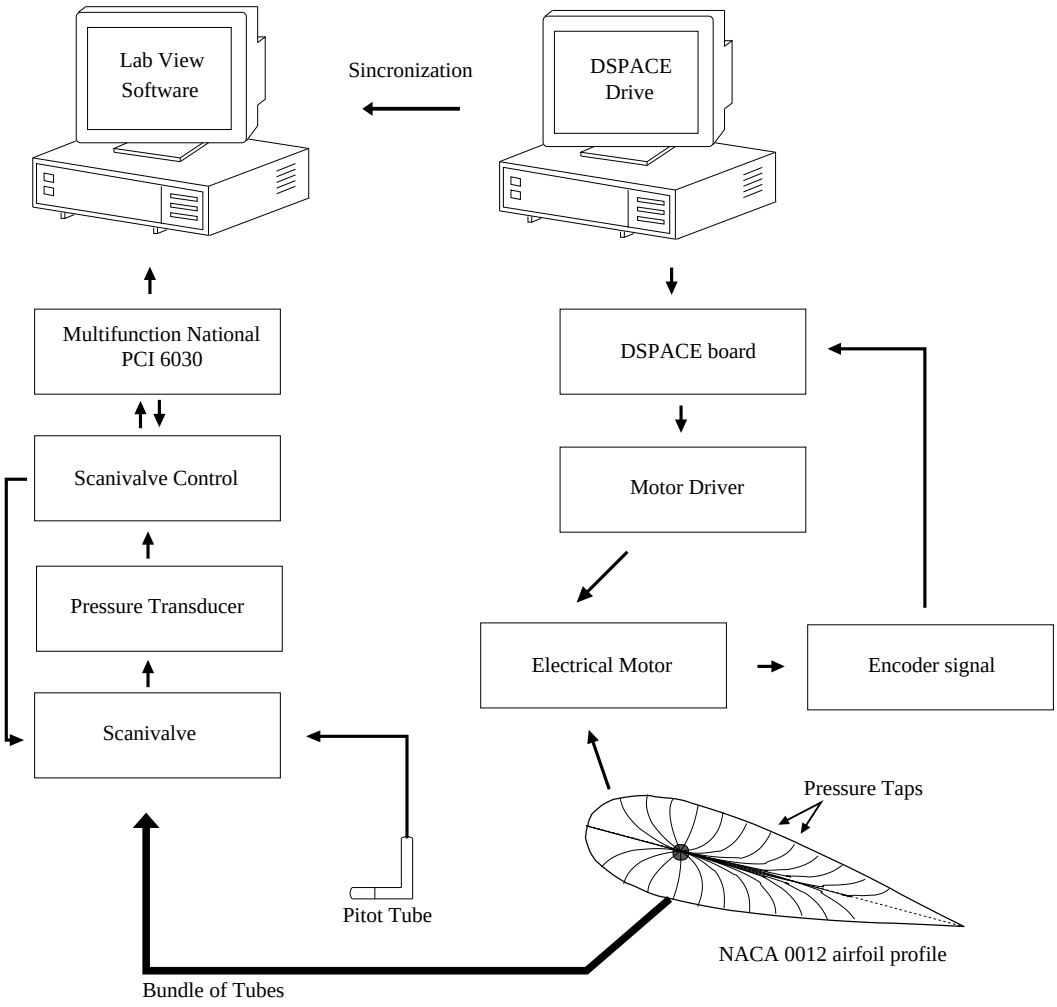

Figure 2. Test setup.

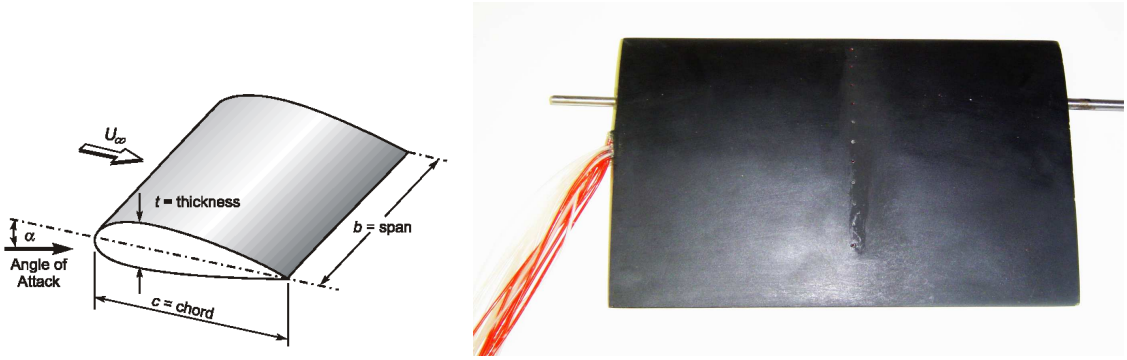

Figure 3. NACA0012 profile model used in this study.

with a 16 bits AD card converter, model PCI 6030 supplied by NI. The acquisition frequency was set to provide a total of 256 samples per oscillation cycle of the airfoil. The equation of data reduction for the pressure coefficient Cp and U_∞ are given by:

$$Cp[(p_i - p_\infty),\ \rho(T),\ U_\infty] = \frac{2(p_i - p_\infty)}{\rho U_\infty^2}, \quad U_\infty = \sqrt{\frac{2(p_{stagn} - p_\infty)}{\rho}},$$

where p_i is the pressure on the model surface measured at location i on the airfoil surface, p_∞ is the static pressure at the testing chamber, ρ is the air density, T is the temperature and p_{stagn} is the total pressure measured with a Pitot that was placed at the entrance of the testing chamber.

An electrical DC motor Nema 23 BRUSHL with an amplifier TD50-2315B and a control unit were used to provide controlled oscillation on the airfoil angle of incidence. The angular movement of the motor was directly transmitted to the airfoil by an elastic coupler connected to a steel rod. This rod was fixed to the airfoil at one quarter of its chord-length. The movement of the motor was driven by a digital PID controller which was emulated by Matlab routines. The signal from an incremental encoder provided the feedback response requested to supply the controller. The communication between the control routines, the amplifier and the encoder was done with a DSPACE multifunction system. The mean incidence angle of the airfoil was set to 15^o and a sinusoidal angular oscillation of 15^o was imposed. Therefore, the incidence angle varied from 0^o to 30^o. Special care was taken in order to synchronize the pressure acquisition with the airfoil oscillation. Ensemble average techniques were used to reduce the influence of non-deterministic noise on the experimental data. In the current experiments the data was ensemble averaged through 15 oscillation cycles of the airfoil.

2.2 COMPUTATIONAL PROCEDURE

Consider compressible homogeneous and inviscid flow in a two-dimensional rectangular domain Ω with an immersed boundary as a simple closed curve Γ, represented by $\mathbf{X}(s,t)$, with $0 \leq s \leq L_b$ and with $\mathbf{X}(0,t) = \mathbf{X}(L_b,t)$, and Lagrangian variables represented by capital letters. The governing equations can be given by:

$$\frac{\partial \mathbf{V}}{\partial t} + \frac{\partial \mathbf{E}}{\partial x} + \frac{\partial \mathbf{G}}{\partial y} = \mathbf{H}\,, \tag{1}$$

where:

$$\mathbf{V} = \begin{bmatrix} \rho \\ \rho u \\ \rho v \\ \rho e \end{bmatrix} \quad \mathbf{E} = \begin{bmatrix} \rho u \\ \rho u^2 + p \\ \rho uv \\ (\rho e + p)\,u \end{bmatrix} \quad \mathbf{G} = \begin{bmatrix} \rho v \\ \rho uv \\ \rho v^2 + p \\ (\rho e + p)\,v \end{bmatrix} \quad \mathbf{H} = \begin{bmatrix} 0 \\ f_1 \\ f_2 \\ u f_1 + v f_2 \end{bmatrix} \tag{2}$$

$$p = (\gamma - 1)\left(\rho e - \frac{1}{2}\rho\left(u^2 + v^2\right)\right)\,, \tag{3}$$

$$\mathbf{f}(\mathbf{x},t) = \int_0^{L_b} \mathbf{F}(s,t)\delta^2(\mathbf{x} - \mathbf{X}(s,t))ds\,, \tag{4}$$

$$\frac{\partial \mathbf{X}(s,t)}{\partial t} = \mathbf{U}(\mathbf{X}(s,t),t) = \int_\Omega \mathbf{u}(\mathbf{x},t)\delta^2(\mathbf{x} - \mathbf{X}(s,t))d\mathbf{x}\,, \tag{5}$$

$$\mathbf{F}(s,t) = \mathbf{S}(\mathbf{X}(s,t),t)\,. \tag{6}$$

In Eq. (1)-(6), $\mathbf{x} = (x,y)$ is the location vector, $\mathbf{u}(\mathbf{x},t) = (u(\mathbf{x},t), v(\mathbf{x},t))$ is the fluid velocity field, $p(\mathbf{x},t)$ is the pressure field, $\rho(\mathbf{x},t)$ is the density field and $e(\mathbf{x},t)$ is the total energy, given by:

$$e = e_i + \frac{1}{2}\left(u^2 + v^2\right)\,, \tag{7}$$

where e_i is the specific internal energy. The force actuating over the fluid is given by $\mathbf{f}(\mathbf{x},t) = (f_1(\mathbf{x},t), f_2(\mathbf{x},t))$, while the force actuating over the immersed boundary is given by $\mathbf{F}(s,t) = (F_1(s,t), F_2(s,t))$. Equation (3) represents the state equation for pressure considering termally perfect gas with $\gamma = 1.4$, and Eq. (6) expresses the elasticity of the boundary. The numerical method used in this paper is given by Doricio and Greco Jr (2007). For the numerical method, C_p was calculated by:

$$C_p = \frac{\frac{p_i - p_\infty}{p_\infty}}{\frac{1}{2}\gamma M_\infty^2}\,,$$

were p_i is the surface pressure measured at location i on the airfoil surface, p_∞ is the pressure in the free-stream, $\gamma = 1.4$, and M_∞ is the free-stream Mach number. Even though compressibility effects are negligible for the present study, the code choice was done based on its availability and interest in testing it for unsteady conditions.

3. RESULTS

The experiments, and the computational simulations, were performed with angle of attack varied from 0^o to 30^o for frequencies of $0.5Hz$ and $2Hz$. The pressure coefficient distribution, for all cases, is used to show the features of the dynamic stall. The computational domain is 6×3 non-dimensional units (a.u.) and the NACA0012 airfoil has chord $c = 1a.u.$ (125 mesh cells). The mesh for the computational simulation has 231 divisions in x direction and 248 divisions in y direction with variable spacement, $\Delta_{xmin} = 0.008$ and $\Delta_{ymin} = 0.004$. The computational simulation was performed with no-reflecting walls based on Riemann invariants (Buonomo, 2004). The rotation center is located at $1/4$ of the airfoil profile chord (the same of used for wind tunnel tests). The oscillating mechanism produced a sinusoidal perturbation (in Fig. 4) and shows a satisfactory agreement between the encoder signal and the theoretical sinusoidal function for frequency of $0.5Hz$. However Fig. 4b shows a significant difference between the encoder and the sinusoidal function for frequency of $2Hz$. Apparentely motor torque was insufficient for the $2Hz$ frequency. This error was ignored due to the mainly qualitative nature of the present analysis.

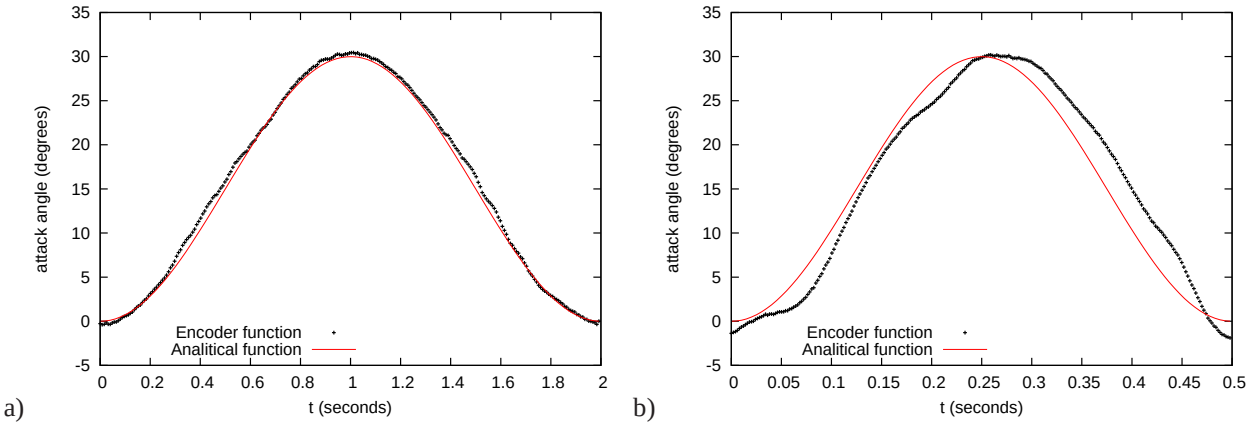

Figure 4. Encoder sinusoidal perturbation: a) 0.5 Hz, b) 2 Hz.

A trailing edge stall appears for all the tests, as shown by analysis of the upper surface pressure plot (Fig. 5 to Fig. 8). It can be noted in Figures 5 to 8 that the stall occurs where the pressure coefficient increases. For example, in Fig. 5 the phenomena occurs about 16.5^o and in Fig. 7 about 22^o. The computational simulation exhibited stall characteristics too, Fig. 6 and Fig. 8, although differences in the shape of the surface pressure variation around the maximum value of pressure coefficient. This can be noted by the comparison between the experimental and computational results for $0.5Hz$ (Fig. 5 and Fig. 6), and $2Hz$ (Fig. 7 and Fig. 8).

The comparison between the computational simulation and the test shows C_p peak with same magnitude. The experimental results to $0.5Hz$ presents maximum C_p peak for attack angle of 16.5^o and recovery C_p peak for attack angle of 14^o. The computational results, for this case, present maximum C_p peak in the 24^o and recovery C_p peak for attack angle of 14^o, see Fig. 5 and Fig. 6. The experimental results to $2.0Hz$ presents maximum C_p peak for attack angle of 22^o and recovery C_p peak for attack angle of 6^o. The computational results present maximum C_p peak in the 28^o and recovery C_p peak for attack angle of 12^o, see Fig. 7 and Fig. 8. This effect, probably, occurred due to absence of viscosity in the computational simulation. The interval of stall phenomenon in the test, for $0.5Hz$, is greater that in the computational one due, probably, to the boundary layer effect. The range of C_p pitching is similar in the experimental and computational results until the attack angle of static stall. The C_p recovery in the pricking is greater in the experimental results than in the computational results, see Fig. 5 and Fig 6. The computational results for $2Hz$ present dynamic stall effect more accented and the phenomenon with the same magnitude, see Fig. 7 and Fig. 8, however the recovery suffers dumping because the numerical method consider inviscid and compressive flow.

The Immersed Boundary Method generates the dynamic effect of recirculation, as shown in Fig. 9 which presents the airfoil in six instants of simulation. Figure 9 presents the airfoil position with attack angle of 15^o, 21^o, 30^o, 19^o, 15^o, and 0^o associated with some angles of the Fig. 8. The dynamic stall occurs at the maximum amplitude (30^o). It can be noted, for the angle of 30^o, that the stall showed by Fig. 8 is represented in Fig. 9 by the vortex formed by the stream line.

Figures 10 and 11 present the normal force coefficient C_N for $0.5Hz$ and $2Hz$. Comparing the experimental with the computational results, the hysteresis is greater in computational results than in experimental results. Absence of viscosity or others factors in the numerical method can be the responsible factors for this different hysteresis effect. These figures also show the experimental result for C_N in stationary regime. This result is very close to the experimental result for non-stationary regime with frequency of $0.5Hz$ up to 20^o. This phenomenon occurs due to low frequency imposed on the airfoil motion. For frequency of $2Hz$ the difference is more intense because of the dynamic stall.

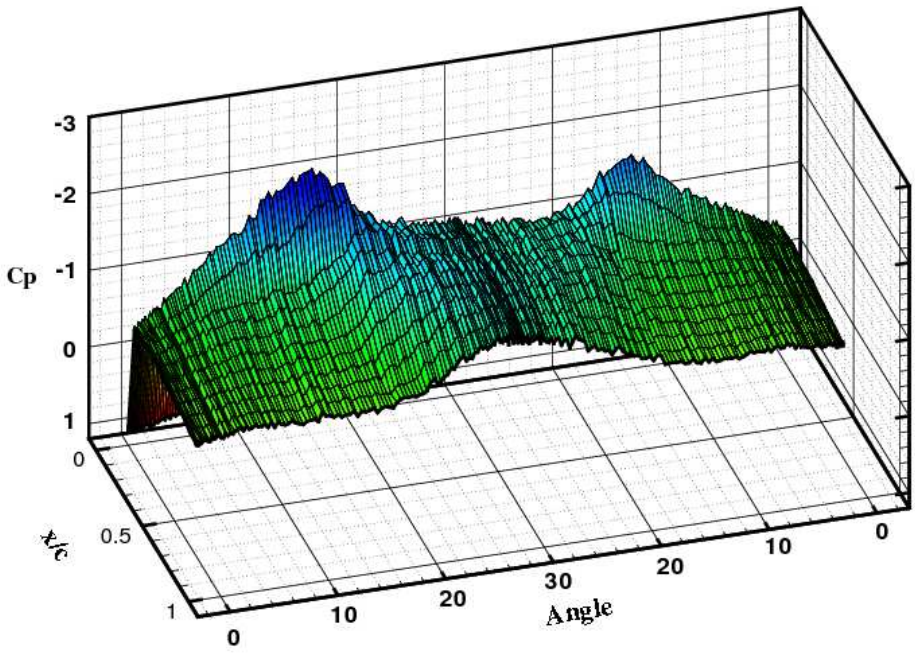

Figure 5. Upper surface pressure for 0.5 Hz-experimental.

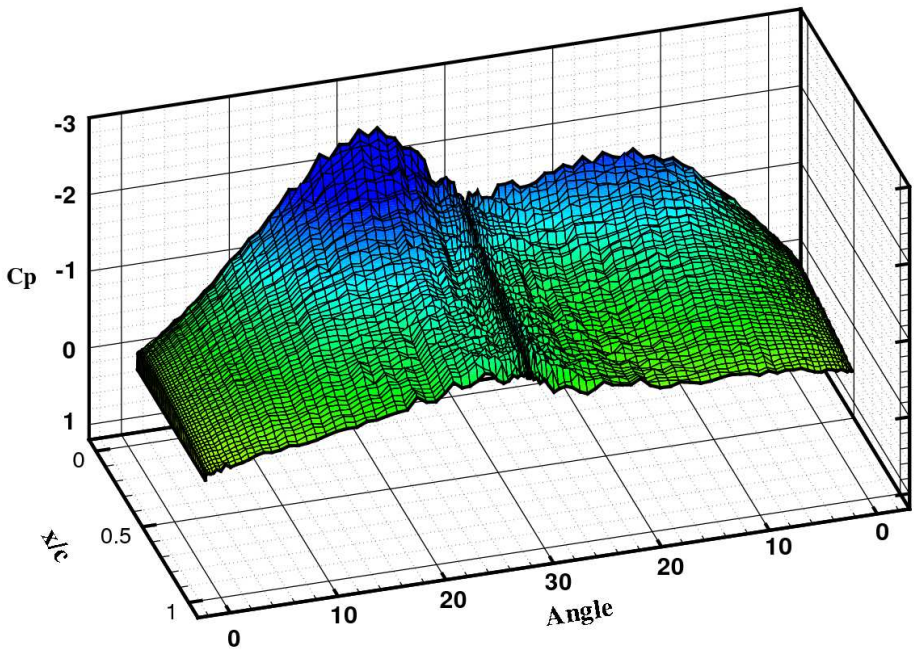

Figure 6. Upper surface pressure for 0.5 Hz-computational.

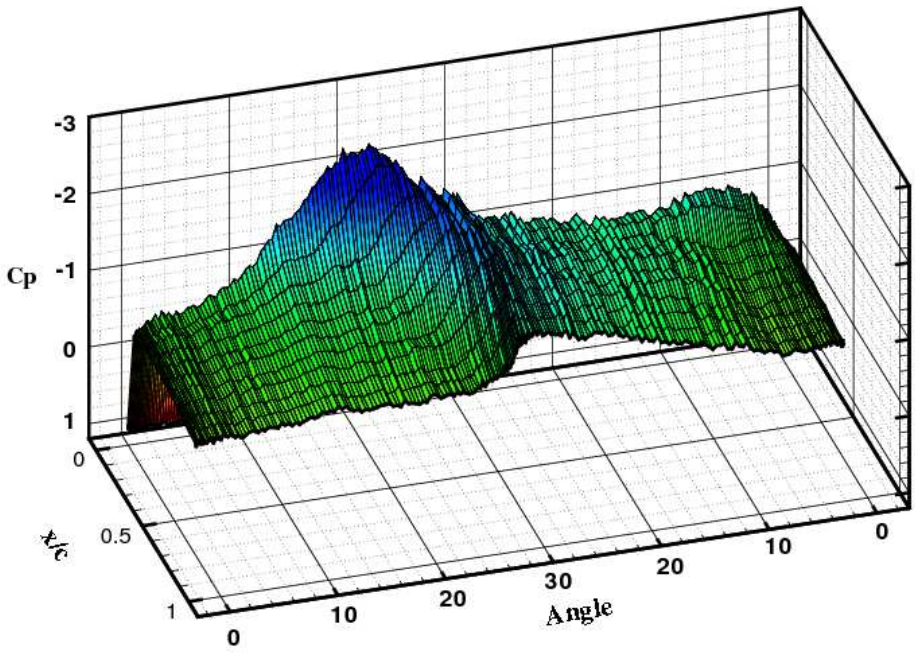

Figure 7. Upper surface pressure for 2 Hz-experimental.

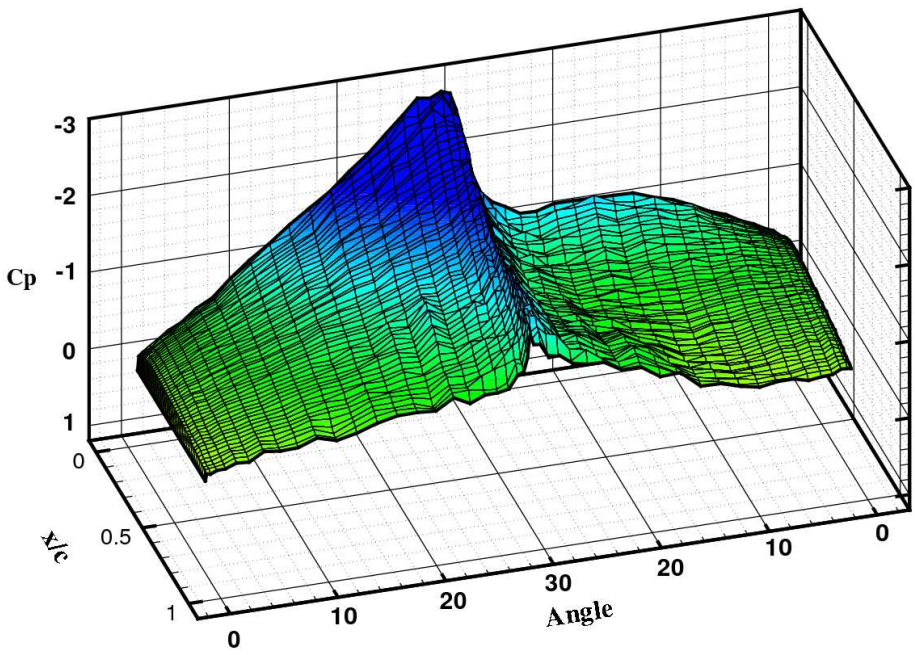

Figure 8. Upper surface pressure for 2 Hz-computational.

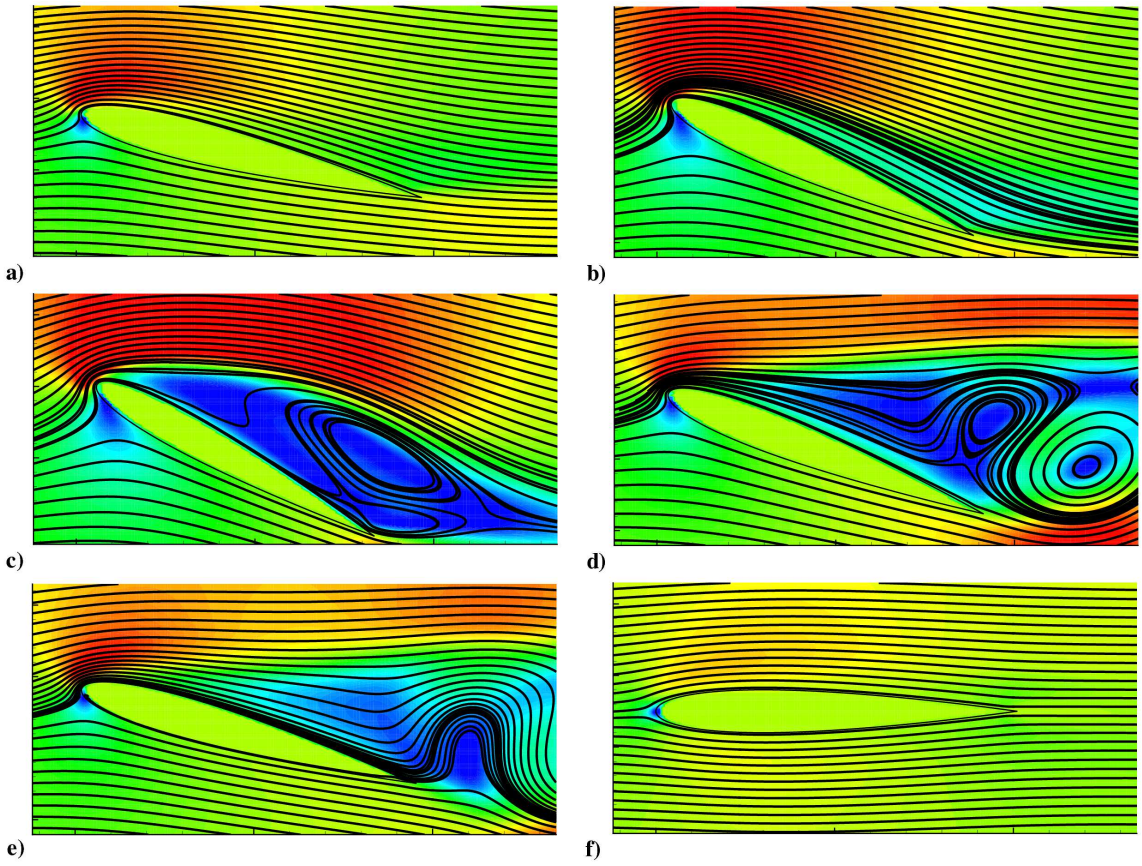

Figure 9. Computational simulation details including the stream lines: a) 15^o, b) 21^o, c) 30^o, d) 19^o, e) 15^o, and f) 0^o.

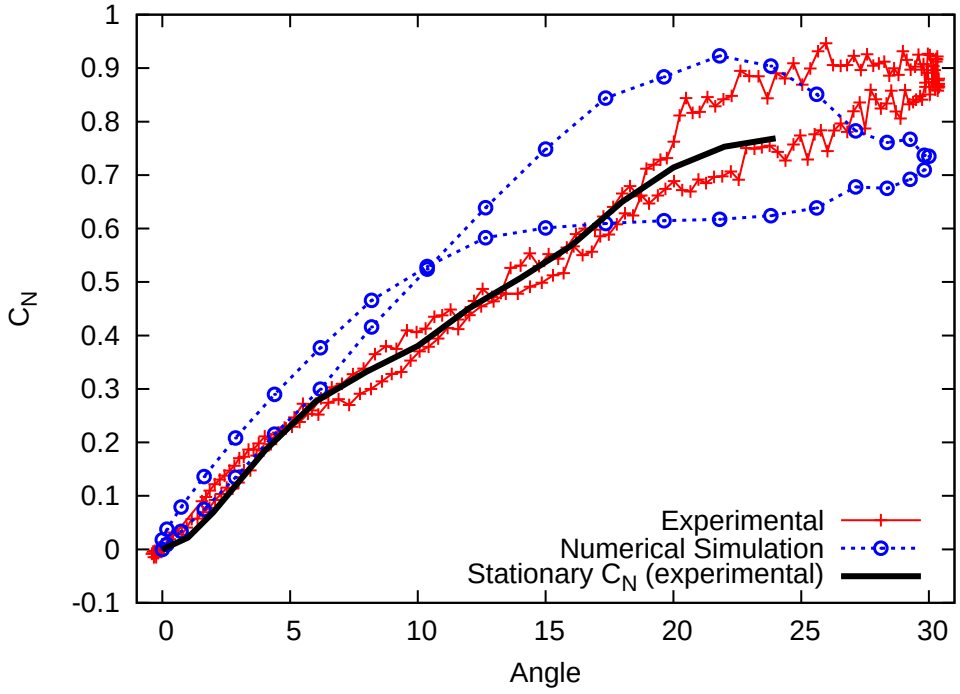

Figure 10. C_N comparison between the experimental and computational results for 0.5 Hz.

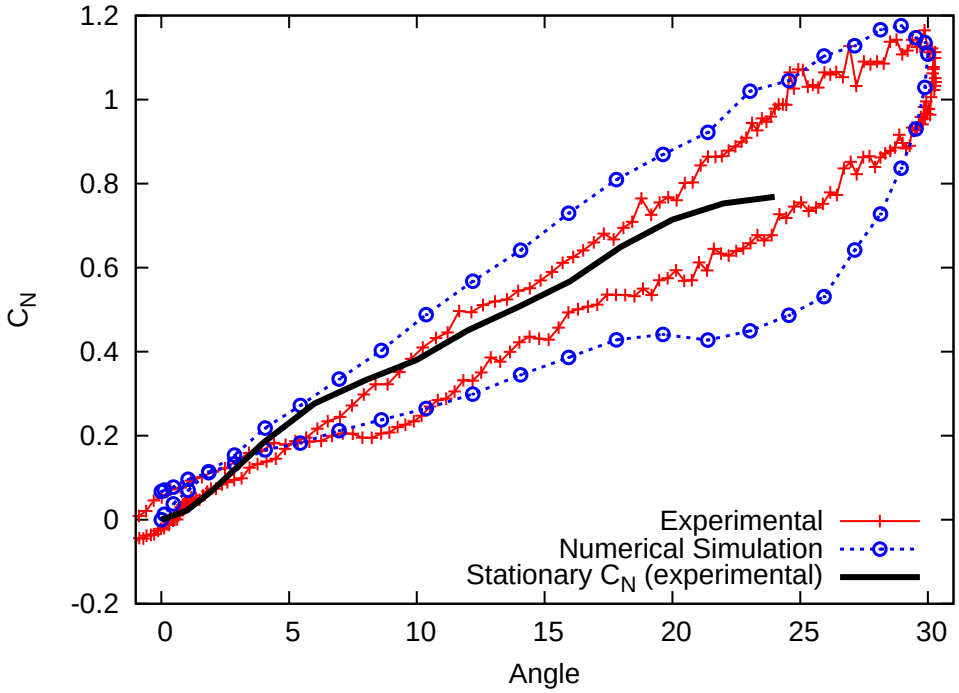

Figure 11. C_N comparison between the experimental and computational results for 2 Hz.

4. CONCLUSIONS

A comparison between the tests and the computational simulations indicated an alternative computational method to study dynamic stall without viscous effects. It was observed that the model reproduce the stall phenomenon as well as it does for airfoil tested at others researchers (Carta, 1974), (Coton and Galbraith, 1999), and (McCroskey et al., 1976), although the experimental parameters are different. Analysis of the wind tunnel data showed that the stall behavior occurs as theoretically expected (Niven and Galbraith, 1997). It must be noted that no wall correction was applied to the experimental results. The motivation behind the computational simulation was to analyze unsteady results using the free-slip Immersed Boundary technique (Doricio and Greco Jr, 2007). The computational results qualitatively agreed with experimental results, despite the lack of viscosity and the very low Mach number ($\cong 0.059$). Also, the stall features in the computational model present two-dimensional behavior, but the details of the stalling process in the wind tunnel present three-dimensional effect.

5. ACKNOWLEDGEMENTS

The authors are thankful for the financial support of CNPQ (Conselho Nacional de Desenvolvimento Científico e Tecnológico) 141051/2006-0.

6. REFERENCES

Barton, J. T. and Pulliam, T. H. 1984. Airfoil Computation at High Angles of Attack, Inviscid and Viscous Phenomena. In AIAA Paper, volume 84-0524.

Buonomo, C. A. 2004. Técnica de Fronteiras Imersas com Formulação Viscosa e Compressível. Master's thesis, Instituto Tecnológico de Aeronáutica.

Carta, F. O. 1974. Analysis of oscillatory pressure data including dynamic stall efects. NASA, CR-2394.

Coton, F. N. and Galbraith, R. A. M. 1999. An experimental study of dynamic stall on a finite wing. The Aeronautical Journal, 103(1023):229–236.

Doricio, J. L. and Greco Jr, P. C. 2007. Free-slip approach of the Immersed Boundary Method. In Proceedings of COBEM 2007, pages 1–8. ABCM.

Filippone, A. and Sorensen, J. N. 1995. A viscous-invicid interaction model for rotor aerodynamics. AGARD Aerodynamics and Aeroacoustics of Rotorcraft. *www.aerodym.org*.

Kumar, A. and Salas, M. D. 1985. Euler and Navier-Stokes solutions for supersonic shear flow past a circular cylinder. AIAA Journal, 83(4):583–587.

Marconi, F. 1983. The spiral singularity in supersonic inviscid flow over a cone. In AIAA Paper, volume 83-1665.
McCroskey, W. J., Carr, L. W., and Mclister, K. W. 1976. Dynamic stall experiments on oscillating airfoils. AIAA Journal, 14(1):57–63.
Niven, A. J. and Galbraith, R. A. M. 1997. Modelling dynamic stall vortex inception at low Mach numbers. The Aeronautical Journal, (2163):67–76.
Raj, P. and Sikora, J. S. 1984. Free-vortex flows: recent encounters with an Euler code. In AIAA Paper, volume 84-0135.

7. Responsibility notice

The authors are the only responsible for the printed material included in this paper.